AQUA
Water Infrastructure, Ecosystems and Society

IWA PUBLISHING

 AQUA — Water Infrastructure, Ecosystems and Society Vol 72 No 4, 411 doi: 10.2166/aqua.2023.178

Comparative study of the adsorptive removal of reactive yellow 14 azo dye from an aqueous solution on different synthetic materials

Sanaa El Aggadi *, Mariem Ennouhi, Younes Kerroum and Abderrahim El Hourch

Materials Nanotechnologies and Environment Laboratory, Department of Chemistry, Faculty of Sciences, Mohammed V University in Rabat, Avenue Ibn Battouta, BP:1014, Rabat, Morocco
*Corresponding author. E-mail: sanaa_elaggadi@um5.ac.ma

SE, 0000-0003-4306-4824; YK, 0000-0003-2146-6515

ABSTRACT

The purpose of this study is to investigate the adsorption behavior of the Reactive Yellow 14 (RY14) azo dye from an aqueous solution onto silica gel (SG), alumina (AO) and powdered activated carbon (PAC) via batch adsorption technique at room temperature (25 °C). Physicochemical properties of the adsorbents were characterized by means of scanning electron microscopy (SEM) coupled with energy-dispersive X-ray spectroscopy (EDS) and X-ray diffraction (XRD). The factors influencing the adsorption of SG, AO and PAC, such as adsorbent dosage, pH, ionic strength, contact time and initial concentration, were conducted to evaluate the adsorption performance. The kinetic studies indicated that the adsorption of RY14 on SG and PAC can be very well fitted by a pseudo-second-order kinetic model, and onto AO by a pseudo-first-order kinetic model. The equilibrium data were best described by a Langmuir model for all adsorbents. The maximum estimated adsorption capacity was 124.6, 116.2 and 200.7 mg·g^{-1}, for SG, AO and PAC, respectively.

Key words: adsorption mechanism, azo dyes, isotherm, kinetics, reactive yellow 14, water treatment

HIGHLIGHTS

- Removal of RY14 azo dye from an aqueous solution onto SG, AO and PAC adsorbents.
- The adsorption of RY14 on SG and PAC was well fitted by a pseudo-second-order kinetic model, whereas the adsorption was fitted by a pseudo-first-order kinetic model on AO.
- The maximum adsorption capacity was 124.6, 116.2 and 200.7 mg·g^{-1}, for SG, AO and PAC, respectively.

INTRODUCTION

Worldwide, the increase in dye pollution problems has become a critical challenge to environmental and biological safety. The main source of dye pollution is industrial wastewater, in particular synthetic dyes used in the textile, printing, brewery, leather, electroplating and pulp industries (El Aggadi *et al.* 2021). Azo dyes account for 50–70% of the dyes used in textile wastewater. It has been shown that this kind of dye has two functional groups: the chromophore (C = C, N = N, C = O) and the auxochrome (–OH, –NH_2, NR_2). The simple azo dyes such as picric acid and the cationic and anionic dyes have no strong bond with cotton fibers because they have hydroxyl groups in their structure and are therefore not appropriate for dyeing these fibers and large amounts of these dyes enter the wastewater (Malek *et al.* 2020). Azo groups are bonded to benzene and naphthalene rings, but in some cases, they are bonded to aliphatic and heterocyclic groups. The number of azo groups defines the index number of the dye. Similarly, solubility and adhesion to fibers are determined by the structure of the chromophore. Within these types of amino groups, the hydroxyl, carboxyl and sulfonic radicals and their derivatives are the factors that bind the dyes to the fibers (Yuan *et al.* 2016). Most azo dyes are toxic and carcinogenic, mutagenic and teratogenic, resulting in serious toxicity to aquatic organisms and destruction of natural ecology (Lum *et al.* 2020). Their removal from aquatic systems becomes an emergency condition. Until now, there are many methods used to remove dyes from polluted waters, such as biodegradation (Gurav *et al.* 2021), electrocoagulation (Özyonar *et al.* 2020), ozonation (Larouk *et al.* 2017), photocatalytic oxidation (Govindan *et al.* 2019) and membrane separation (Li *et al.* 2019a). Fan *et al.* (2012) have stated that adsorption is considered a

successful, attractive approach and now it is considered to be superior to other techniques for water treatment in terms of initial cost, the wide availability of adsorbents, high efficiency, ease of use, simplicity of design and reusability.

The aim of this investigation is to test the adsorption behavior of Reactive Yellow 14 (Table 1) azo dye in an aqueous solution on silica gel (SG), alumina (AO) and powdered activated carbon (PAC). The dye was chosen as the adsorbate for the present study because it is widely used in the textile industry. Additionally, this dye belongs to the group of azo dyes, which are mainly carcinogenic, mutagenic and toxic, causing skin irritation, allergies, dermatitis, cancer and mutations in humans and animals (Konicki *et al.* 2017). We selected these three adsorbents based on their large availability, low cost and high specific area. The adsorbents were characterized by scanning electron microscopy (SEM) coupled with energy-dispersive X-ray spectroscopy (EDS) and X-ray diffraction (XRD). Moreover, the influence of experimental conditions such as adsorbent dosage, pH, ionic strength, contact time and initial concentration was investigated through the use of batch experiments. The adsorption kinetics and isotherms of the azo dye RY14 were also evaluated by different models to better understand the adsorption mechanism.

MATERIALS AND METHODS

Materials

Commercially available SG SiO_2 (70–200 μm, 60 Å pore diameter) was purchased from MEGA SCIENCE. Aluminium oxide or alumina Al_2O_3 was purchased from Fluka (type 507 C, neutral, 100–125 mesh, pH = 7). Commercial PAC was provided by PICA Charbon Actif company. RY14 dye ($C_{20}H_{19}ClN_4Na_2O_{11}S_3$, molar mass: 669 g·mol^{-1}) was purchased from Sigma-Aldrich and used without further purification. Sulfuric acid and sodium hydroxide of analytical grade were purchased from Sigma-Aldrich. Chemicals used in this work were all reagent grade and were used with no further purification. All solutions were prepared using deionized water.

Characterization of adsorbents

The surface morphologies of SG, alumina (AO) and PAC adsorbents were characterized by JEOL JSM-IT 100 (Tokyo, JAPAN) SEM coupled with EDS. The structure of samples was characterized by XRD (LABXXRD-6100 SHIMADZU, Columbia, United States) using Kα radiation ($\lambda = 1.5406$ Å) in the 2θ range of 10°–70°. The X-ray tube was operated at 40 kV with a Cu target.

Adsorption experiments

In order to determine the adsorption performances, a comparative study was conducted for the removal of RY14 using SG, AO and PAC as adsorbents. The effect of adsorbent dose on the RY14 dye removal was investigated using an aqueous solution containing 100 mg·L^{-1} RY14 dye at natural pH (6.3) and various adsorbent dosages ranging between 0.5 and 5 g·L^{-1}.

Table 1 | The chemical structure and characteristics of Reactive Yellow 14 (RY14)

Dye name	C.I. Reactive Yellow 14 (RY14)
Group	Azo class
Molecular formula	$C_{20}H_{19}ClN_4Na_2O_{11}S_3$
Molecular weight	669 g·mol^{-1}
λ_{max}	410 nm
Structure	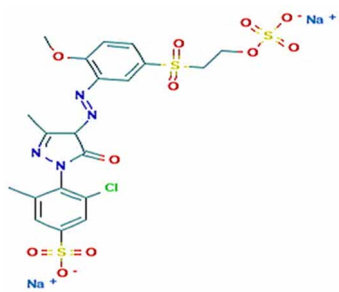

To study the effect of pH on dye adsorption, 0.025 g of adsorbent was added to 25 mL of 100 mg·L^{-1} RY14 solutions at various pH values ranging from 3 to 10. The pH of the aqueous solution was adjusted using 0.1 M H_2SO_4 or 0.1 M NaOH solutions. Initial RY14 dye concentration of 100 mg·L^{-1} and 1 g·L^{-1} of adsorbent was used. The aqueous solutions were shaken for 2 h.

The effect of ionic strength was investigated using Na_2SO_4, KCl and KNO_3 in different concentrations (0.01–0.5 M). In order to do a kinetic study, adsorption experiments were conducted as follows: 0.025 g of adsorbent was suspended in 25 mL solution containing 100 mg·L^{-1} of RY14 dye. Then, all the sealed flasks were shaken at different time intervals. Equilibrium isotherm experiments were carried out at room temperature (25 °C), whereby 0.025 g of adsorbent was added to 25 mL of RY14 solutions of varying concentrations (0–200 mg·L^{-1}). After filtration, the concentration of RY14 in the filtrate was determined with an ultraviolet-visible spectrophotometer (Analytik Jena, Specord 210 plus) and the adsorption amount Q_e (mg g^{-1}) of the sample was calculated by using the following formula (Feng *et al.* 2020):

$$Q_e = \frac{(C_0 - C_e) * V}{m}$$

where C_0 and C_e are the initial and equilibrium dye concentration (mg·L^{-1}), respectively, V is the volume of solution (L) and m is the mass of absorbent (g).

RESULTS AND DISCUSSION

Characterization of adsorbents

SEM equipped with EDS analysis was used to directly observe the microstructural characteristics and confirm the compositions of SG, AO and PAC particles. As displayed in Figure 1(a), it is apparent that the surface of SG is relatively smooth, clear and has an irregular shape. The EDS showed that the tested SG samples contained no impurities. Similar results were previously reported (Bityukov *et al.* 2018). Irregular shapes and agglomerated particles, as well as clear, sharp edges with silts appeared for the AO particles (Figure 1(b)). EDS analysis showed that the main elements found are O and Al, which indicates the high purity of AO particles (Ahmad *et al.* 2016). PAC particles (Figure 1(c)) are both agglomerated and dispersed. The edges of the grains are angular while the surface is rough and porous. Visible pores can be observed on the edges and surface of PAC grains. The results of the EDS spectra show that 82.96 wt % of the sample was carbon, 15.26 wt % was oxygen and 1.79 wt % of the remaining elements was the total of the weight % of Mg, Si and Ca (Li *et al.* 2019c).

Figure 2 shows the XRD diffractogram of SG, AO and PAC. The XRD plot of SG (Figure 2(a)) showed a broad peak in 2θ value of 21.80°. The width of the peak indicates the amorphous nature of SG. The AO XRD (Figure 2(b)) peaks at $2\theta = 31.92°$, 37.60°, 45.79° and 67.3° correspond to the reflection from the (220), (311), (400) and (440) planes. The maximum diffraction peaks observed were characteristic of γ-Al_2O_3, showing that the AO was mainly composed of γ-Al_2O_3. Nevertheless, many other metastable AOs, called transition aluminas, present similar XRD traces, which makes phase identification more complicated (Sifontes *et al.* 2014). XRD patterns of PAC (Figure 2(c)) exhibited three intense peaks at 26.6°, 37.7° and 44°. We can see that the material is well crystallized with the presence of an amorphous part. Similar findings have been previously reported (Selvaraju & Bakar 2017).

Adsorption experiments

Effect of adsorbent dosage: the effect of adsorbent dosage on the removal efficiency of RY14 by SG, AO and PAC was tested by varying the adsorbent dose from 0.5 to 5 g·L^{-1} for the dye concentration of 100 mg·L^{-1} at natural pH (6.3), as shown in Figure 3. The result shows that the adsorption capacity increases with increasing adsorbent dose, after a certain dose of adsorbent, the maximum adsorption is reached and thus the amount of dye bound to the adsorbent and the amount of free dye remain constant even after adding the amount of adsorbent. This can be attributed to the formation of aggregates at higher solid/liquid ratios or to the sedimentation of particles (Fakhri 2017). For 1 g·L^{-1} adsorbent dose, about 40.21 mg·g^{-1}, 89.78 mg·g^{-1} and 81.06 mg·g^{-1} of RY14 can be removed with SG, AO and PAC, respectively. This was caused by the increase in adsorbent surface area and the availability of more adsorption sites of the adsorbent (Idan 2017). The adsorbent dose of 1 g·L^{-1} was chosen for all adsorbents in further studies.

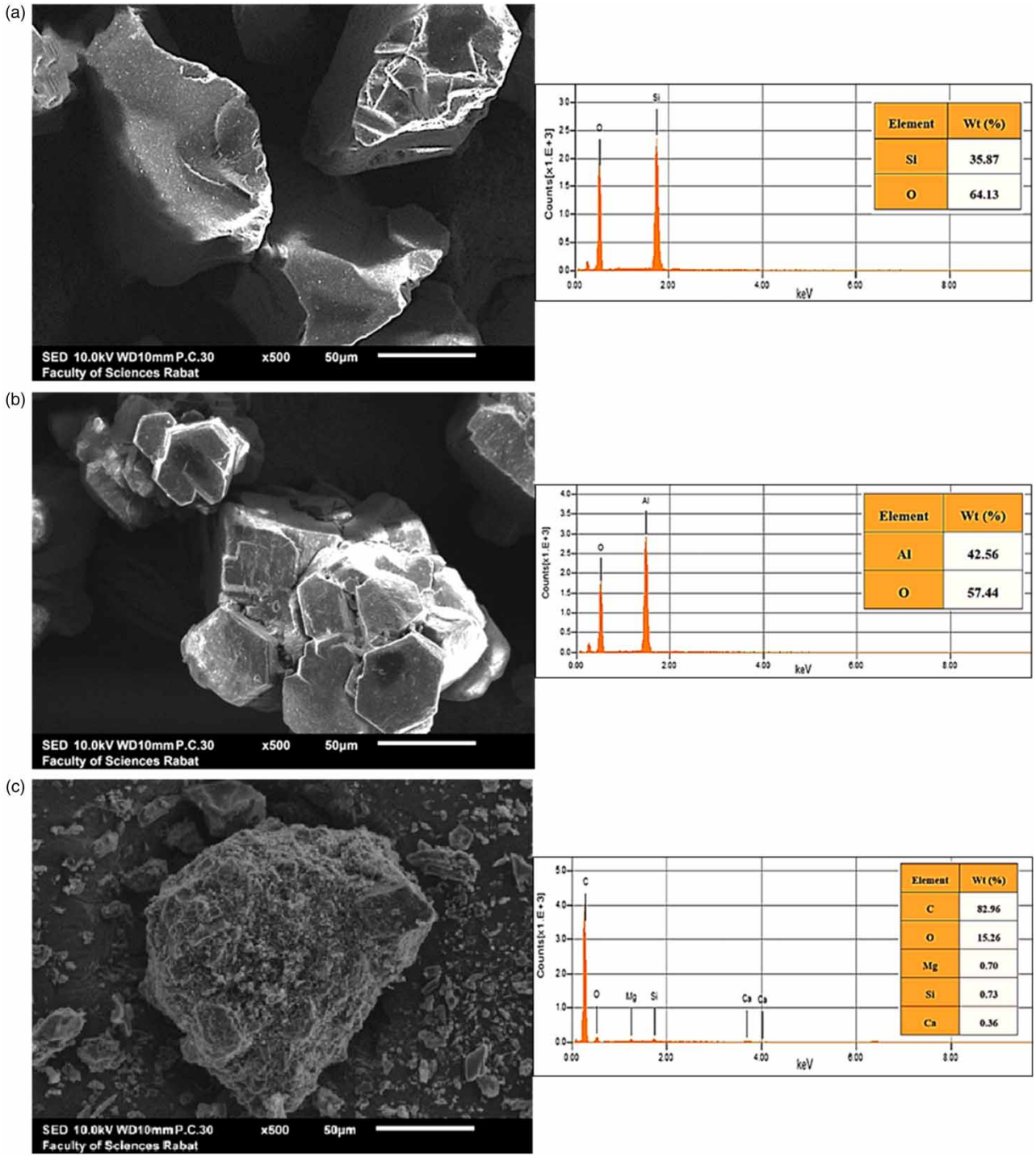

Figure 1 | SEM micrographs and EDS spectra of (a) SG, (b) AO and (c) PAC.

Effects of initial solution pH: we investigated the effect of pH on the adsorption process by undertaking the batch adsorption procedure at various hydrogen ion concentrations by keeping the other parameters constant. The initial pH of the adsorption media was varied between 3 and 10 (Figure 4). It can be seen that for PAC, the influence of pH on the adsorption capacity of adsorbed RY14 is weak, the amount of RY14 adsorbed at equilibrium decreases slowly from 92.02 to 84.17 $mg{\cdot}g^{-1}$ as the pH increases from pH 3–10, while SG and AO were strongly influenced by hydrogen ion concentrations. It was found

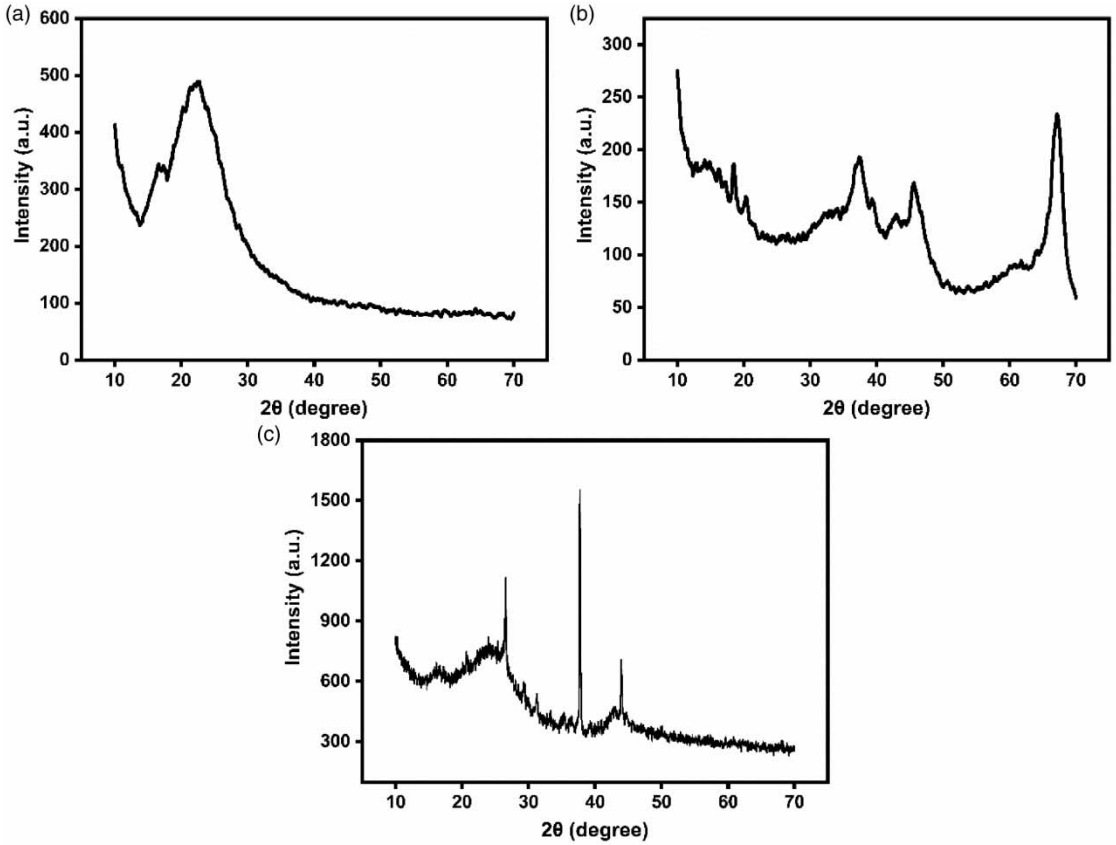

Figure 2 | The XRD patterns of (a) SG, (b) AO and (c) PAC.

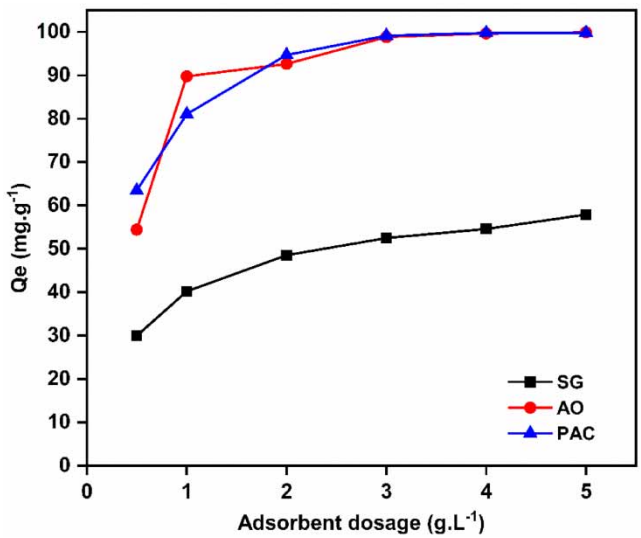

Figure 3 | Effect of adsorbent dosage on adsorption capacity of RY14 (Conditions: $C_0 = 100$ mg·L^{-1}, time = 6 h, pH = 6.3, $T = 25$ °C).

that when the pH increases from 3 to 10, the adsorption capacity decreased from 66.59 to 35.95 mg·g^{-1} for SG and from 99 to 32.05 mg·g^{-1} for AO. It is speculated that this was due to the presence of an excess of OH^- ions competing with RY14 for the hydrogen bond formed with the adsorbents coordinated water molecules in the interlayer (Fakhri 2017).

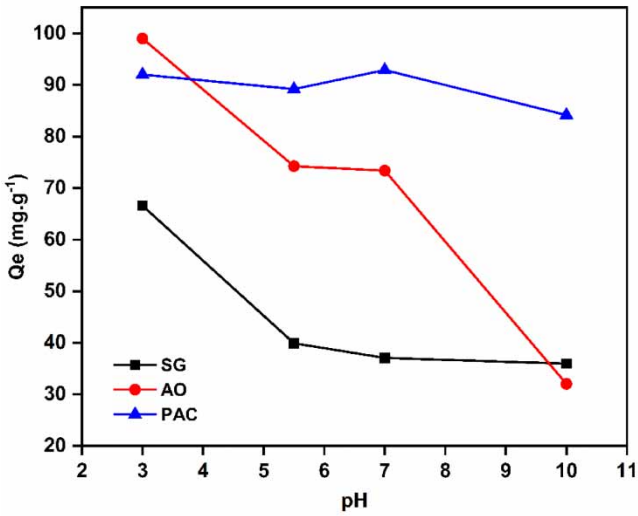

Figure 4 | Effect of initial pH on adsorption capacity of RY14 (Conditions: $C_0 = 100$ mg·L^{-1}, time = 2 h, adsorbent dose = 1 g·L^{-1}, $T = 25$ °C).

Effect of ionic strength: The presence of salt in water results in a high ionic strength, which can affect the efficiency of the adsorption process (Eren 2009). Na_2SO_4, KNO_3 and KCl salts in concentration ranges of 0.01–0.5 M were added to the aqueous solutions of dye to investigate the effect of ionic strength on dye adsorption. As shown in Figure 5, the adsorption capacity of RY14 increases for all three adsorbents after the addition of 0.05 M salt concentration, but any increase in a salt concentration above 0.05 M has little influence on the dye adsorption; a slight increase in the adsorption capacity of RY14 can be observed. The maximum capacity was obtained with the KCl salt for SG and PAC. However, the highest capacity was obtained with both KNO_3 and KCl salts for AO. These results suggest that the presence of an additional electrolyte, such as Na_2SO_4, KNO_3 and KCl, has a limited effect on the binding efficiency between adsorbent and RY14 dye. A similar behavior was observed for methylene blue dye at kaolinite clay–water (Mukherjee *et al.* 2015) and also methyl blue adsorption on poly(4-vinylpyridine)–graphene oxide–Fe_3O_4 magnetic nanocomposites (Li *et al.* 2019b).

Adsorption kinetics modeling

The effect of contact time on the adsorption capacity of RY14 dye using SG, AO and PAC as adsorbents is shown in Figure 6. The absorption of RY14 increases strongly after the first minutes and reaches saturation after 60 min for both SG and AO as well as after 20 min for PAC. Adsorption was faster at the beginning, which may be due to the availability of the uncovered surface of the adsorbents (Aljeboree *et al.* 2017). Nevertheless, the active sites were progressively occupied by the dye molecules and a decrease in the adsorption sites of the remaining dye molecules in the solution was observed over time. This finding demonstrates the advantages of using these inexpensive adsorbents for the treatment of aqueous solutions charged with dyes in general and RY14 in particular.

The kinetics of the adsorption process of RY14 on SG, AO and PAC was investigated by fitting the experimental adsorption data using the nonlinear forms of the pseudo-first-order, pseudo-second-order and Elovich models (Henning *et al.* 2019), as depicted in Figure 6(a)–6(c).

$$Q_t = Q_e(1 - e^{-K_1 t}) \quad \text{Pseudo-first-order}$$

$$Q_t = \frac{K_2\, Q_e^2 t}{1 + K_2 Q_e t} \quad \text{Pseudo-second-order}$$

$$Q_t = \frac{1}{\beta} \ln(\alpha\beta t + 1) \quad \text{Elovich}$$

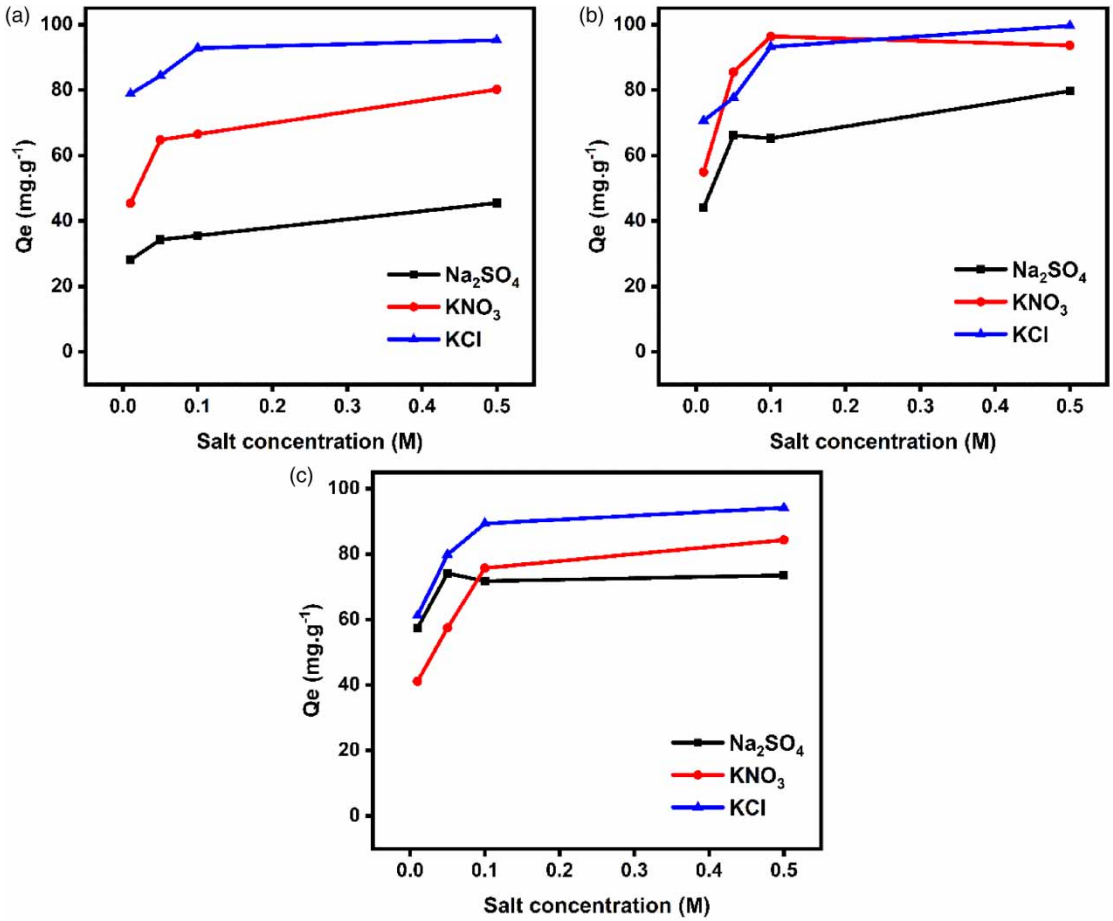

Figure 5 | Effect of ionic strength on adsorption capacity of RY14 by (a) SG, (b) AO and (c) PAC (Conditions: $T = 25$ °C; adsorbent dose = 1 g·L^{-1}; $C_0 = 100$ mg·L^{-1}; time = 30 min).

where Q_e (mg·g^{-1}) and Q_t (mg·g^{-1}) are the adsorption capacities at equilibrium and at time t (min), respectively. K_1 (min^{-1}) and K_2 (g·mg^{-1}·min^{-1}) are the pseudo-first-order rate constant and the pseudo-second-order rate constant, respectively. α (mg·g^{-1}·min^{-1}) and β (g·mg^{-1}) are the initial adsorption rate constant and the desorption rate, respectively.

The corresponding kinetic parameter values calculated from the pseudo-first-order, pseudo-second-order and Elovich models are presented in Table 2, and the kinetic model plots are displayed in Figure 6(a)–6(c). A comparison of the results with the correlation coefficients indicates that the pseudo-second-order model is the best-fitting model for experimental kinetics data of SG, and the theoretical adsorption capacity Q_e(cal) of the pseudo-second-order kinetic model was closer to the experimental measured value Q_e(exp), suggesting possible chemisorption occurring between RY14 molecules and SG adsorbent (Chen *et al.* 2020). The higher regression coefficient ($R^2 = 0.99$) also suggests that the adsorption of RY14 on AO follows pseudo-first-order kinetics. Additionally, the value of the calculated Q_e matches perfectly the experimental data and this further confirms the best applicability of the pseudo-first-order model. For PAC adsorbent, although both the R^2 values of the pseudo-first-order model and the pseudo-second-order model correlate well with the experimental data, the Elovich model with the high initial adsorption rate $\alpha = 1.37 \times 10^{20}$ mg·g^{-1}·min^{-1} clearly indicated that the pseudo-second-order model best fit the adsorption kinetics of RY14 on PAC. Moreover, the theoretical adsorption capacity Q_e(cal) of the pseudo-second-order kinetic model was closer to the experimentally measured value Q_e(exp).

Identification of the adsorption process is crucial to develop the best adsorption system, as well as for the prediction of the rate-limiting step (Bhaumik *et al.* 2016). Adsorption dynamics included three consecutive steps. The first stage is the boundary diffusion, in which the adsorbate diffuses on the adsorbent external surface. The second stage is the intraparticle diffusion into

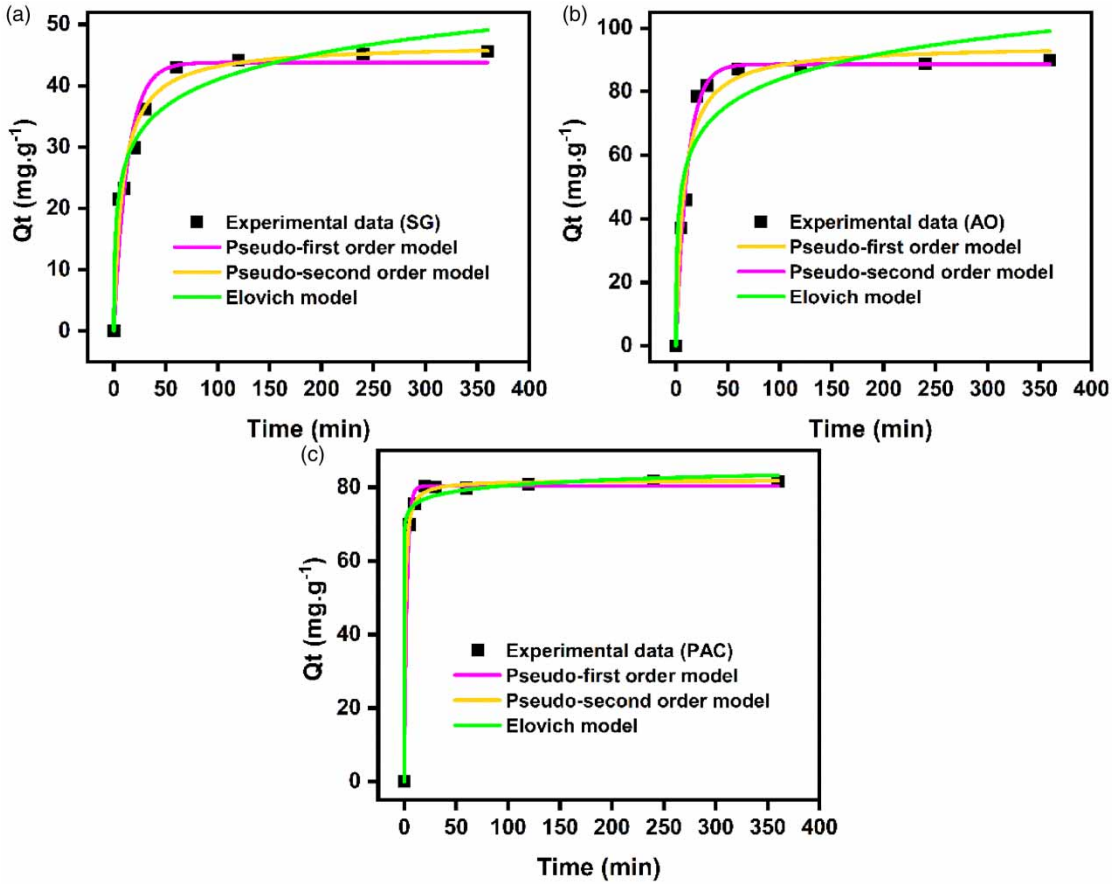

Figure 6 | Experimental data of adsorption kinetic and nonlinear fitting of pseudo-first-order, pseudo-second-order and Elovich models for RY14 adsorption onto (a) SG, (b) AO and (c) PAC (Conditions: $C_0 = 100$ mg·L^{-1}, $T = 25$ °C, pH = 6.3, $V = 25$ mL, adsorbent dose = 1 g·L^{-1}).

Table 2 | Parameters for pseudo-first-order, pseudo-second-order and Elovich kinetic models for RY14 adsorption

Models	Parameter	SG	AO	PAC
Pseudo-first-order	Q_e (exp) (mg·g^{-1})	44.5	87.55	81.9
	Q_e (cal) (mg·g^{-1})	43.79	88.6	80.37
	K_1 (min^{-1})	0.07	0.09	0.39
	R^2	0.95	0.99	0.99
Pseudo-second-order	Q_e (exp) (mg·g^{-1})	44.5	87.55	81.9
	Q_e (cal) (mg·g^{-1})	46.01	94.65	81.96
	K_2 (g·mg^{-1}·min^{-1})	0	0	0.01
	R^2	0.98	0.97	0.99
Elovich	α (mg·g^{-1}·min^{-1})	42.22	140.46	$1.82.10^{13}$
	β (g·mg^{-1})	0.16	0.08	0.44
	R^2	0.96	0.9	0.99

the pores of the adsorbent. The third stage is the adsorbate being adsorbed in the inner sites of the adsorbent. The Weber and Morris (Weber & Morris 1963) intraparticle diffusion model was used to investigate the rate-limiting step of RY14 adsorption.

$$Q_t = K_p t^{1/2} + C$$

where K_p (mg g^{-1} min$^{-1/2}$) is the intraparticle diffusion rate constant and C (mg·g^{-1}) is the intercept which is proportional to the thickness of the boundary layer (Sielser 1977).

If plotting Q_t versus $t^{1/2}$, we get a straight line through the origin, in this case, intraparticle diffusion is the only step controlling the rate. In contrast, the adsorption process was controlled by two or more steps (Boparai *et al.* 2011).

The curves of Q_t versus $t^{1/2}$ for different RY14 adsorbents are shown in Figure 7. The plots show three straight lines indicating that three steps took place. The high values of K_{p1} presented in Table 3 reveal that in the first stage, diffusion of RY14 from solution to the outer surface of the adsorbent is immediate and then slowed down within 6 h ($K_{p3} < K_{p2} < K_{p1}$). The fast adsorption is mainly attributed to boundary layer diffusion or diffusion in macropores, and the slow adsorption is caused by intraparticle diffusion or diffusion in micropores (Pan *et al.* 2017). Such a finding is similar to that made in previous studies (Li *et al.* 2019c; Yuan *et al.* 2019).

Adsorption isotherm

Adsorption isotherm analysis is of basic importance in describing how adsorbate molecules interact with the adsorbent surface. Equilibrium studies determine the capacity of the adsorbent and depict the adsorption isotherm by constants giving information about the surface properties and affinity of the adsorbents (Sen *et al.* 2011). Figure 8 shows the adsorption

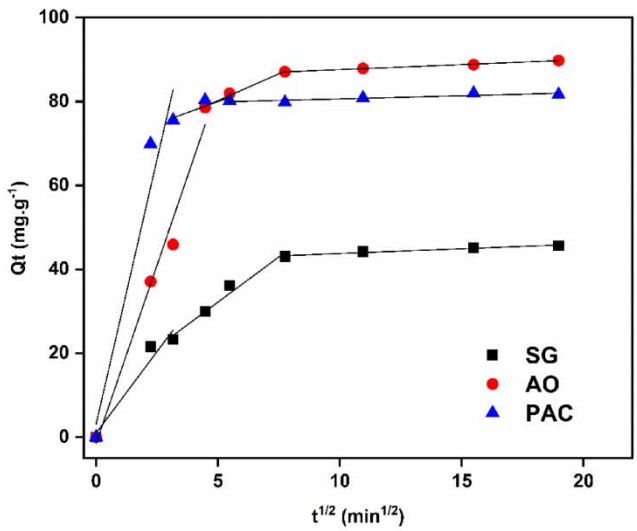

Figure 7 | Intraparticle diffusion models for RY14.

Table 3 | Intraparticle diffusion model parameters for the adsorption of RY14

Stage	Parameter	SG	AO	PAC
1	K_{p1} (mg·g^{-1}·min$^{-1/2}$)	7.77	16.97	25.23
	C_1 (mg·g^{-1})	0	0	0
	R^2	0.98	0.99	0.96
2	K_{p2} (mg·g^{-1}·min$^{-1/2}$)	4.31	2.56	2.1
	C_2 (mg·g^{-1})	10.6	67.42	69.49
	R^2	0.97	0.99	0.9
3	K_{p3} (mg·g^{-1}·min$^{-1/2}$)	0.23	0.24	0.15
	C_3 (mg·g^{-1})	41.48	85.21	79.13
	R^2	0.98	0.99	0.91

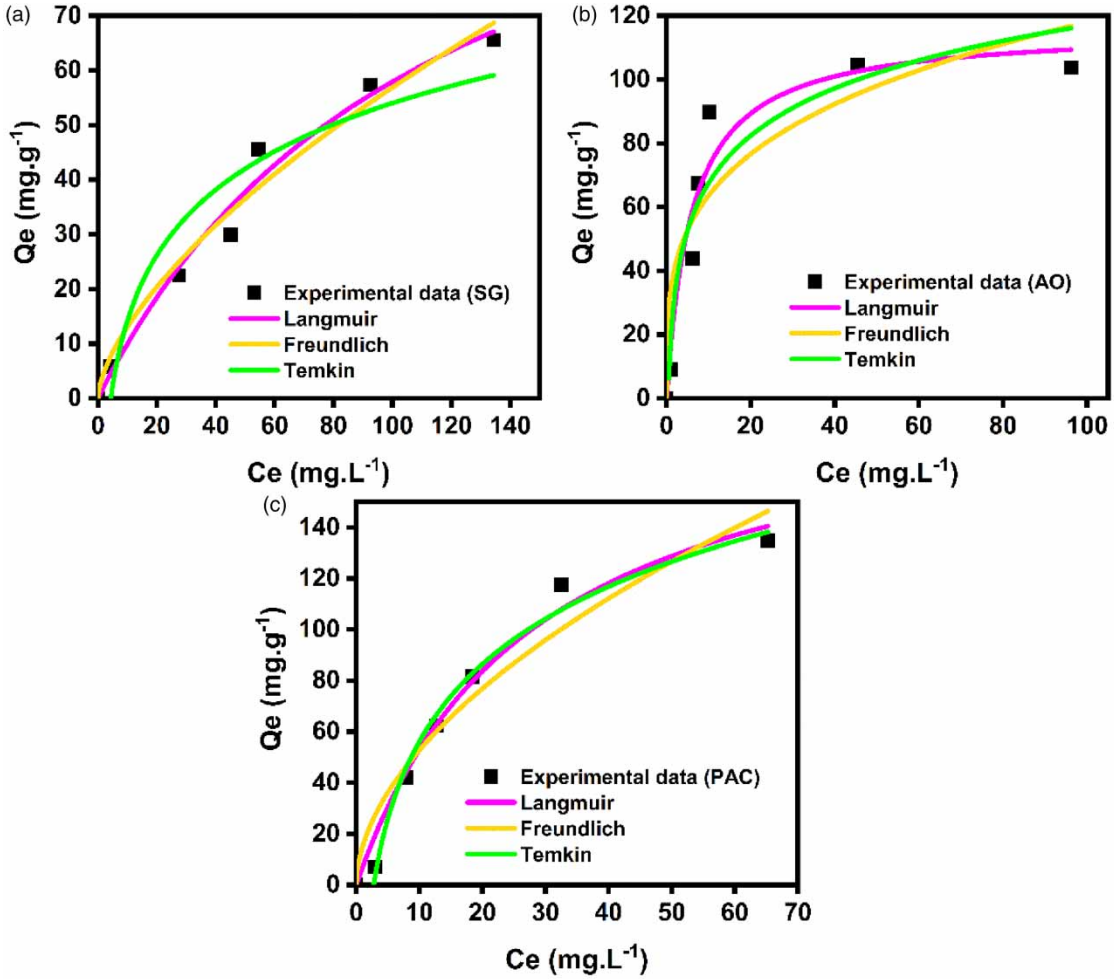

Figure 8 | Adsorption isotherms fitting at different initial concentrations for RY14 adsorption on (a) SG. (b) AO and (c) PAC (Conditions: pH = 6.3; $T = 25$ °C; $V = 25$ mL; time = 6 h; adsorbent dose = 1 g·L^{-1}).

isotherms of RY14 dye on SG, AO and PAC over a concentration range of 0–200 mg·L^{-1}. The nonlinear forms of the Langmuir, Freundlich and Temkin isotherm models were used to analyze the RY14 dye removal equilibrium data. Differences between linear and nonlinear regressions have often found that the best parameter estimates are obtained by nonlinear optimizations (Ho 2004; Boulinguiez *et al.* 2008).

Langmuir isotherm: The Langmuir adsorption isotherm (Langmuir 1916) supposes that monolayer adsorption occurs on an adsorbent with a structurally homogeneous surface, on which the binding sites have the same affinity for adsorption, and that there is no interaction between the molecules adsorbed on neighboring sites. The Langmuir model can be represented as:

$$Q_e = \frac{Q_m K_L C_e}{1 + K_L C_e}$$

where Q_e (mg·g^{-1}) is the adsorption capacity of the adsorbent at equilibrium, Q_m (mg·g^{-1}) is the maximum adsorption capacity, C_e (mg·L^{-1}) is the concentration of the dye solution at equilibrium and K_L (L·mg^{-1}) is the Langmuir equilibrium adsorption constant related to the energy of adsorption which quantitatively reflects the affinity between the adsorbent and adsorbate.

Freundlich isotherm: The Freundlich isotherm (Freundlich 1906) is an empirical equation describing that the adsorption occurs on an energetically heterogeneous surface, on which the adsorbed molecules are interactive and the adsorption

capacity is dependent on the concentration of the adsorbate at equilibrium. The Freundlich equation is expressed as:

$$Q_e = K_F\, C_e^{1/n}$$

K_F (L g^{-1}) is the Freundlich constant related to adsorption capacity and $1/n$ is the intensity of the adsorption or surface heterogeneity indicating the relative distribution of the energy and the heterogeneity of the adsorbate sites.

Temkin isotherm: The Temkin isotherm (Temkin 1940) is based on the hypothesis that the free energy of adsorption depends on the surface coverage and considers the interactions between adsorbents and adsorbed. The nonlinear form of Temkin isotherm has the following expression:

$$Q_e = \left(\frac{RT}{b}\right)\ln(K_T\, C_e)$$

where K_T is the equilibrium binding constant (L·g^{-1}), b is Temkin constant related to heat of adsorption (J·mol^{-1}), R is the universal gas constant (8.314·J·mol^{-1}·K^{-1}) and T is the absolute temperature (K).

The amounts of RY14 (Q_e) adsorbed against C_e are shown in Figure 8. The parameters obtained from the nonlinear equations of each model are presented in Table 4. For the system studied, the Langmuir isotherm correlates best with the experimental data of the adsorption equilibrium of the RY14 dye by the SG, AO and PAC adsorbents, suggesting a monolayer adsorption. Additionally, the degree of suitability of the adsorbent to the RY14 dye was evaluated from the values of the separation factor constant (R_L), which has historically been used to indicate whether the adsorption is favorable or not. The value of R_L will indicate whether the type of isotherm is irreversible ($R_L = 0$), favorable ($0 < R_L < 1$), linear ($R_L = 1$) or unfavorable ($R_L > 1$), which can be calculated from the following equation (Yi *et al.* 2017):

$$R_L = \frac{1}{1 + K_L C_0}$$

where K_L is the Langmuir constant and C_0 is the highest initial dye concentration (mg·L^{-1}). The R_L values of these three adsorbents are greater than zero and less than unity, which suggests that the adsorption processes between adsorbents and RY14 are favorable. The maximum adsorption capacities obtained by Langmuir isotherm model of SG, AO and PAC for RY14 dye are 124.6, 116.2 and 200.7 mg·g^{-1}, respectively. Moreover, according to the correlation coefficient ($R^2 = 0.99$), the results show that the Temkin isotherm also has a strong affinity for the adsorption capacity of RY14 on PAC. Similar findings have also been reported by other researchers (Schimmel *et al.* 2010). Comparison of the adsorption capacity of azo dyes onto adsorbents is presented in Table 5.

CONCLUSIONS

This study demonstrates that SG, AO and PAC materials are effective adsorbents for eliminating RY14 azo dye from aqueous solutions. The amount of RY14 dye uptake was found to increase with increase in amount of adsorbent, ionic strength, contact time and initial dye concentration. But it was found to decrease with increase in the initial solution pH. Based on the

Table 4 | The fitting parameters of adsorption isotherms for RY14 adsorption

Isotherm models	Parameter	SG	AO	PAC
Langmuir	Q_m (mg·g^{-1})	124.6	116.2	200.7
	K_L (L·mg^{-1})	0.01	0.17	0.04
	R^2	0.98	0.95	0.98
Freundlich	K_F (mg·g^{-1})	3	34.25	15.05
	$1/n$	0.64	0.27	0.47
	R^2	0.97	0.85	0.94
Temkin	K_T (L·g^{-1})	0.23	2.31	0.36
	b (J·mol^{-1})	143.13	115.23	56.59
	R^2	0.92	0.92	0.99

Table 5 | Comparison of adsorption capacities for the removal of different azo dyes

Adsorbent	Dye removed	Adsorption capacity (mg/g)	Reference
Hydroxyapatite	Congo Red	139	Bensalah *et al.* (2020)
Graphene oxide	Acid Orange 8 Direct Red 23	29.0 15.3	Konicki *et al.* (2017)
Raw bentonite	Methyl Orange	34.3	Eren (2010)
Activated carbon derived from *Monotheca buxifolia* waste seeds	Eriochrome Black T Remazol Brilliant Blue Remazol Yellow Remazol Brilliant Orange	112.3 96.3 97.6 90.9	Nazir *et al.* (2020)
Coconut mesocarp cellulose modified with CTAC	Congo Red	18.4	Tejada-Tovar *et al.* (2021)
KOH-activated polypyrrole-based adsorbent	Methyl Orange	520.8	Alghamdi *et al.* (2019)
Cornulaca monacantha	Congo Red	43.4	Manirethan *et al.* (2019)
Zirconium-based Chitosan	Orange II	926	Zhang *et al.* (2015)
Polyaniline	Tartrazine	434.5	Sahnoun & Boutahala (2018)
Nanosized SnO_2	Congo Red	48.3	Abdelkader *et al.* (2016)
Silica gel	Reactive Yellow 14	124.6	This work
Alumina	Reactive Yellow 14	116.2	This work
Powdered activated carbon	Reactive Yellow 14	200.7	This work

kinetic studies, the adsorption of RY14 on SG and PAC was found to be very well fitted by a pseudo-second-order kinetic model, whereas the adsorption was fitted by a pseudo-first-order kinetic model on AO. The adsorption data are in good agreement with the Langmuir isotherm, with a maximum monolayer adsorption capacity of 124.6, 116.2 and 200.7 $mg{\cdot}g^{-1}$ for SG, AO and PAC, respectively. The high adsorption capacity of SG, AO and PAC makes them promising adsorbents for industrial applications and environmental protection.

DATA AVAILABILITY STATEMENT

All relevant data are available from an online repository or repositories.

CONFLICT OF INTEREST

The authors declare there is no conflict.

REFERENCES

Abdelkader, E., Nadjia, L. & Rose-Noëlle, V. 2016 Adsorption of Congo red azo dye on nanosized SnO_2 derived from sol-gel method. *International Journal of Industrial Chemistry* **1** (7), 53–70.

Ahmad, W., Al-Matar, A., Shawabkeh, R. & Rana, A. 2016 An experimental and thermodynamic study for conversion of CO_2 to CO and methane over Cu-K/Al_2O_3. *Journal of Environmental Chemical Engineering* **4** (3), 2725–2735.

Alghamdi, A. A., Al-Odayni, A.-B., Saeed, W. S., Almutairi, M. S., Alharthi, F. A., Aouak, T. & Al-Kahtani, A. 2019 Adsorption of azo dye methyl orange from aqueous solutions using alkali-activated polypyrrole-based graphene oxide. *Molecules* **24** (20). doi:10.3390/MOLECULES24203685.

Aljeboree, A. M., Alshirifi, A. N. & Alkaim, A. F. 2017 Kinetics and equilibrium study for the adsorption of textile dyes on coconut shell activated carbon. *Arabian Journal of Chemistry* **10**, S3381–S3393.

Bensalah, H., Younssi, S. A., Ouammou, M., Gurlo, A. & Bekheet, M. F. 2020 Azo dye adsorption on an industrial waste-transformed hydroxyapatite adsorbent: kinetics, isotherms, mechanism and regeneration studies. *Journal of Environmental Chemical Engineering* **8** (3), 103807.

Bhaumik, M., Agarwal, S., Gupta, V. K. & Maity, A. 2016 Enhanced removal of Cr(VI) from aqueous solutions using polypyrrole wrapped oxidized MWCNTs nanocomposites adsorbent. *Journal of Colloid and Interface Science* **470**, 257–267.

Bityukov, O. V., Vil, V. A., Merkulova, V. M., Nikishin, G. I. & Terent'Ev, A. O. 2018 Silica gel mediated oxidative C-O coupling of β-dicarbonyl compounds with malonyl peroxides in solvent-free conditions. *Pure and Applied Chemistry* **90** (1), 7–20.

Boparai, H. K., Joseph, M. & O'Carroll, D. M. 2011 Kinetics and thermodynamics of cadmium ion removal by adsorption onto nano zerovalent iron particles. *Journal of Hazardous Materials* **186** (1), 458–465.

Boulinguiez, B., Le Cloirec, P. & Wolbert, D. 2008 Revisiting the determination of Langmuir parameters-application to tetrahydrothiophene adsorption onto activated carbon. *Langmuir* **24** (13), 6420–6424.

Chen, W., Guo, Y., Mi, X., Yu, Y. & Li, G. 2020 Enhanced adsorptive removal of methylene blue by low-temperature biochar derived from municipal activated sludge. *Desalination and Water Treatment* **188**, 257–265.

El Aggadi, S., El Abbassi, Z. & El Hourch, A. 2021 Color removal from dye-containing aqueous solutions by electrooxidation. *Desalination and Water Treatment* **215**, 232–236.

Eren, E. 2009 Removal of basic dye by modified Unye bentonite, Turkey. *Journal of Hazardous Materials* **162** (2–3), 1355–1363.

Eren, E. 2010 Adsorption performance and mechanism in binding of azo dye by raw bentonite. *CLEAN – Soil, Air, Water* **38** (8), 758–763.

Fakhri, A. 2017 Adsorption characteristics of graphene oxide as a solid adsorbent for aniline removal from aqueous solutions: kinetics, thermodynamics and mechanism studies. *Journal of Saudi Chemical Society* **21**, S52–S57.

Fan, L., Luo, C., Li, X., Lu, F., Qiu, H. & Sun, M. 2012 Fabrication of novel magnetic chitosan grafted with graphene oxide to enhance adsorption properties for methyl blue. *Journal of Hazardous Materials* **215–216**, 272–279.

Feng, C., Ren, P., Li, Z., Tan, W., Zhang, H., Jin, Y. & Ren, F. 2020 Graphene/waste-newspaper cellulose composite aerogels with selective adsorption of organic dyes: preparation, characterization, and adsorption mechanism. *New Journal of Chemistry* **44** (6), 2256–2267.

Freundlich, H. M. 1906 Over the adsorption in solution. *Journal of Physicochemical* **57A** (1), 385–470.

Govindan, K., Suresh, A. K., Sakthivel, T., Murugesan, K., Mohan, R., Gunasekaran, V. & Jang, A. 2019 Effect of peroxomonosulfate, peroxodisulfate and hydrogen peroxide on graphene oxide photocatalytic performances in methyl orange dye degradation. *Chemosphere* **237**, 124479.

Gurav, R., Bhatia, S. K., Choi, T. R., Choi, Y. K., Kim, H. J., Song, H. S., Lee, S. M., Lee Park, S., Lee, H. S., Koh, J., Jeon, J. M., Yoon, J. J. & Yang, Y. H. 2021 Application of macroalgal biomass derived biochar and bioelectrochemical system with *Shewanella* for the adsorptive removal and biodegradation of toxic azo dye. *Chemosphere* **264**, 128539.

Henning, L. M., Simon, U., Gurlo, A., Smales, G. J. & Bekheet, M. F. 2019 Grafting and stabilization of ordered mesoporous silica COK-12 with graphene oxide for enhanced removal of methylene blue. *RSC Advances* **9** (62), 36271–36284.

Ho, Y. S. 2004 Selection of Optimum Sorption Isotherm. *Carbon* **42** (10), 2115–2116.

Idan, I. J. 2017 Adsorption of anionic dye using cationic surfactant-modified kenaf core fibers. *OALib* **04** (07), 1–18.

Konicki, W., Aleksandrzak, M., Moszyński, D. & Mijowska, E. 2017 Adsorption of anionic azo-dyes from aqueous solutions onto graphene oxide: equilibrium, kinetic and thermodynamic studies. *Journal of Colloid and Interface Science* **496**, 188–200.

Langmuir, I. 1916 The constitution and fundamental properties of solids and liquids. Part I. Solids. *Journal of the American Chemical Society* **38** (11), 2221–2295.

Larouk, S., Ouargli, R., Shahidi, D., Olhund, L., Shiao, T. C., Chergui, N., Sehili, T., Roy, R. & Azzouz, A. 2017 Catalytic ozonation of Orange-G through highly interactive contributions of hematite and SBA-16 – to better understand azo-dye oxidation in nature. *Chemosphere* **168**, 1648–1657.

Li, J., Gong, J. L., Zeng, G. M., Zhang, P., Song, B., Cao, W. C., Fang, S.-Y., Huan, S.-Y. & Ye, J. 2019a The performance of UiO-66-NH2/graphene oxide (GO) composite membrane for removal of differently charged mixed dyes. *Chemosphere* **237**, 124517.

Li, Y., Lu, H., Wang, Y., Zhao, Y. & Li, X. 2019b Efficient removal of methyl blue from aqueous solution by using poly(4-vinylpyridine)–graphene oxide–Fe_3O_4 magnetic nanocomposites. *Journal of Materials Science* **54** (10), 7603–7616.

Li, Z., Yang, Y., Jáuregui-Haza, U., Guo, Z. & Campos, L. C. 2019c The impact of humic acid on metaldehyde adsorption onto powdered activated carbon in aqueous solution. *RSC Advances* **9** (1), 11–22.

Lum, P. T., Foo, K. Y., Zakaria, N. A. & Palaniandy, P. 2020 Ash based nanocomposites for photocatalytic degradation of textile dye pollutants: a review. *Materials Chemistry and Physics* **241**, 122405.

Malek, N. N. A., Jawad, A. H., Abdulhameed, A. S., Ismail, K. & Hameed, B. H. 2020 New magnetic Schiff's base-chitosan-glyoxal/fly ash/Fe3O4 biocomposite for the removal of anionic azo dye: an optimized process. *International Journal of Biological Macromolecules* **146**, 530–539.

Manirethan, V., Gupta, N., Balakrishnan, R. M. & Raval, K. 2019 Batch and continuous studies on the removal of heavy metals from aqueous solution using biosynthesised melanin-coated PVDF membranes. *Environmental Science and Pollution Research 2019 27:20* **27** (20), 24723–24737.

Mukherjee, K., Kedia, A., Jagajjanani Rao, K., Dhir, S. & Paria, S. 2015 Adsorption enhancement of methylene blue dye at kaolinite clay-water interface influenced by electrolyte solutions. *RSC Advances* **5** (39), 30654–30659.

Nazir, R., Khan, M., Rehman, R. U., Shujah, S., Khan, M., Ullah, M., Zada, A., Mahmood, N. & Ahmad, I. 2020 Adsorption of selected azo dyes from an aqueous solution by activated carbon derived from *Monotheca buxifolia* waste seeds. *Soil and Water Research* **15** (3), 166–172.

Özyonar, F., Gökkuş, Ö. & Sabuni, M. 2020 Removal of disperse and reactive dyes from aqueous solutions using ultrasound-assisted electrocoagulation. *Chemosphere* **258**, 127325.

Pan, M., Lin, X., Xie, J. & Huang, X. 2017 Kinetic, equilibrium and thermodynamic studies for phosphate adsorption on aluminum hydroxide modified palygorskite nano-composites. *RSC Advances* **7** (8), 4492–4500.

Sahnoun, S. & Boutahala, M. 2018 Adsorption removal of tartrazine by chitosan/polyaniline composite: kinetics and equilibrium studies. *International Journal of Biological Macromolecules* **114**, 1345–1353.

Schimmel, D., Fagnani, K. C., Dos Santos, J. B. O., Barros, M. A. S. D. & Da Silva, E. A. 2010 Adsorption of turquoise blue qg reactive dye on commercial activated carbon in batch reactor: kinetic and equilibrium studies. *Brazilian Journal of Chemical Engineering* **27** (2), 289–298.

Selvaraju, G. & Bakar, N. K. A. 2017 Production of a new industrially viable green-activated carbon from Artocarpus integer fruit processing waste and evaluation of its chemical, morphological and adsorption properties. *Journal of Cleaner Production* **141**, 989–999.

Sen, T. K., Afroze, S. & Ang, H. M. 2011 Equilibrium, kinetics and mechanism of removal of methylene blue from aqueous solution by adsorption onto pine cone biomass of Pinus radiata. *Water, Air, and Soil Pollution* **218** (1–4), 499–515.

Sielser, H. W. 1977 Polymer-solvent interaction: the IR-dichroic behaviour of DMF residues in drawn films of polyacrylonitrile. *Colloid and Polymer Science Kolloid-Zeitschrift & Zeitschrift Für Polymere* **255** (4), 321–326.

Sifontes, Á. B., Gutierrez, B., Mónaco, A., Yanez, A., Díaz, Y., Méndez, F. J., Llovera, L., Cañizales, E. & Brito, J. L. 2014 Preparation of functionalized porous nano-γ-Al_2O_3 powders employing colophony extract. *Biotechnology Reports* **4** (1), 21–29.

Tejada-Tovar, C., Villabona-Ortíz, Á. & Gonzalez-Delgado, Á. D. 2021 Adsorption of Azo-Anionic dyes in a solution using modified coconut (Cocos nucifera) Mesocarp: kinetic and equilibrium study. *Water* **13** (10), 1382.

Temkin, M. J. 1940 Recent modifications to Langmuir isotherms. *Acta Physiochim, URSS* **12**, 217–225.

Weber, W. J. & Morris, J. C. 1963 Kinetics of adsorption on carbon from solution. *Journal of the Sanitary Engineering Division* **82** (2), 31–60.

Yi, X., Xu, Z., Liu, Y., Guo, X., Ou, M. & Xu, X. 2017 Highly efficient removal of uranium(VI) from wastewater by polyacrylic acid hydrogels. *RSC Advances* **7** (11), 6278–6287.

Yuan, B., Qiu, L. G., Su, H. Z., Cao, C.-L. & Jiang, J.-H. 2016 Schiff base – Chitosan grafted l-monoguluronic acid as a novel solid-phase adsorbent for removal of Congo red. *International Journal of Biological Macromolecules* **82**, 355–360.

Yuan, Z., Wang, J., Wang, Y., Liu, Q., Zhong, Y., Wang, Y., Li, L., Lincoln, S. F. & Guo, X. 2019 Preparation of a poly(acrylic acid) based hydrogel with fast adsorption rate and high adsorption capacity for the removal of cationic dyes. *RSC Advances* **9** (37), 21075–21085.

Zhang, L., Chen, L., Liu, X. & Zhang, W. 2015 Effective removal of azo-dye orange II from aqueous solution by zirconium-based chitosan microcomposite adsorbent. *RSC Advances* **5** (114), 93840–93849.

First received 28 May 2021; accepted in revised form 29 October 2021. Available online 3 April 2023